SUPPLEMENT TO THE *WELDING JOURNAL*, MAY 2011
Sponsored by the American Welding Society and the Welding Research Council

Gas Metal Arc Weld Pool Surface Imaging: Modeling and Processing

A reflection-based observation system successfully reduced arc light interference

BY X. MA AND Y. ZHANG

ABSTRACT

Observing and measuring the weld pool geometry in the gas metal arc welding (GMAW) process is the key to understanding and control of a complex welding process. The harsh environment and highly dynamic characteristic of a weld pool surface made the observation extremely challenging. In this paper, a reflection-based GMA weld pool surface observation system is proposed to monitor the three-dimensional weld pool geometry. A low-power five-line laser pattern is projected onto the weld pool and the reflected pattern, which is the result of an intercepted reflected laser beam on an imaging plane, is captured and analyzed. To image the reflected laser pattern, the elements in the imaging system including laser and weld pool surface are analyzed and modeled. The effects of their parameters such as laser density, projection angle, weld pool surface geometry, and weld pool surface fluctuation on the imaging of the laser pattern are examined and analyzed. The effectiveness of the proposed method and parameter ranges are verified through simulation and experiments. As a result, acceptable images of laser pattern reflected from the weld pool surface in pulsed GMAW were acquired. An image processing algorithm has been developed to successfully extract the reflected laser pattern for subsequent weld pool surface reconstruction.

Introduction

Observation of the weld pool provides an effective path to understand and control the welding process. Observation data also attribute to the validation of numerical models, which helps researchers to analyze and evaluate the welding process.

Extensive research has been conducted to provide in situ monitoring of the weld pool. The arc sensor was one of the first few sensors that was adopted for weld pool observation. X-ray (Ref. 1), infrared, and vision-based sensors were also developed and implemented. The weld pool surface is the most direct source of information for human welders to obtain feedback. Skilled welders estimate the welding process by visually observing the weld pool and adjust welding parameters accordingly.

In recent years, machine vision has been more and more widely adopted to monitor the welding process. Early efforts focused on extracting a two-dimensional weld pool boundary by directly viewing the scene under the welding gun. Richardson (Ref. 2) developed a coaxial arc weld pool viewing system for the gas tungsten arc welding (GTAW) process. Kovacevic et al. (Ref. 3) used a high-power auxiliary illumination laser to suppress arc radiation. In recent years, weld pool observation evolved from two-dimensional (2-D) boundary extraction to three-dimensional (3-D) surface geometry measurement. Stereo vision (Ref. 4) and shape from shading (SNF) algorithms (Ref. 5) are proposed to reconstruct 3-D weld pool geometry from directly captured weld pool images.

However, one of the most challenging tasks that direct-viewing vision-based monitoring techniques must overcome is the interference of arc radiation, which degrades the quality of captured images. The radiation from the arc body is much stronger than that radiated/reflected from the weld pool surface and workpiece. A scene, including weld pool and welding arc, contains a lot more variations than can be captured by a high-speed camera. The majority of the dynamics on the captured image is assigned to the bright arc body, which is not the area of interest. The dynamics of the weld pool area are significantly reduced and cause an inevitable loss of information.

The most common techniques that were adopted to reduce arc influence included blocking the arc body using a mechanical method (Ref. 1), using optical filters to observe the weld pool surface at a specific wavelength, and using an auxiliary light source, such as laser (Ref. 3), to suppress arc influence. However, according to current reports, the dynamics of the captured weld pool surface are still not satisfying.

Arc light reflected from the weld pool surface is another issue direct-viewing methods have difficulty in overcoming. In the case of weld pool fluctuation, bright spots, which are a result of arc light reflection, are observed in certain local areas on the weld pool. The reflection is significantly brighter than the average weld pool intensity on the captured image, which degrades the dynamic range of the captured weld pool area. When the weld pool surface is reconstructed using stereo vision or SNF method, surface geometry is calculated from captured texture on the weld pool images. The existence of arc light reflection inevitably degrades the weld pool texture and reduces reconstruction accuracy.

Reflection-based weld pool monitoring methods, which take advantage of the specular nature of the weld pool surface, successfully reduced arc light interference. Pioneering work was conducted at the Uni-

KEYWORDS

Gas Metal Arc
Imaging
Sensor
Weld Pool

X. MA and Y. ZHANG (ymzhang@engr.uky.edu) *are with the Department of Electrical and Computer Engineering, University of Kentucky, Lexington, Ky.*

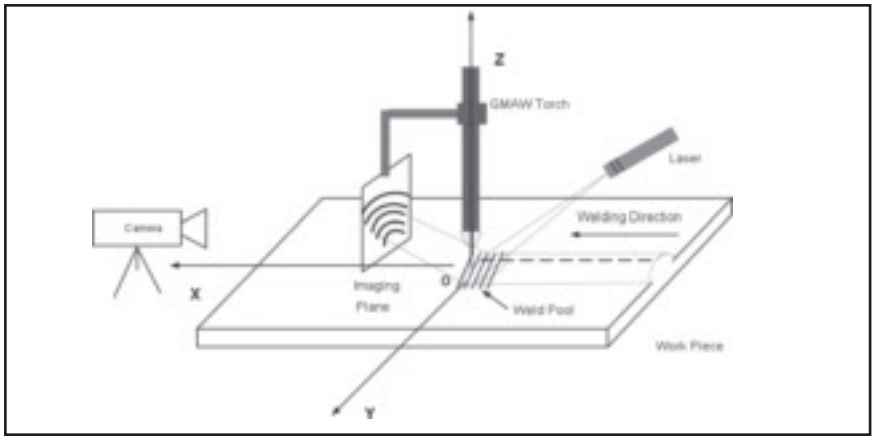

Fig. 1 — System schematic of GMAW-P weld pool observation system.

versity of Kentucky by Kovacevic and Zhang (Ref. 6). The 3-D geometry of the weld pool is extracted by directly viewing the reflection of an illumination laser pattern from the weld pool surface. However, a high-power auxiliary laser is required to generate the laser pattern and suppress the arc light.

Song (Ref. 7) extended this approach by projecting a low-power dot-matrix laser pattern onto the GTA weld pool surface and observing the intercepted reflected laser on an imaging plane. In that application, the weld pool surface is stable with little fluctuation, and the weld pool surface is flat with minor deformation, which can be considered as a special case for the welding process.

Little work was conducted in precisely measuring the 3-D weld pool surface geometry of the gas metal arc welding (GMAW) process. Most current research is based on the direct viewing method, such as shape from shading or stereo vision. In our previous work (Ref. 8), a reflection-based GMA weld pool measuring system was proposed. Weld pool surface monitoring was partially achieved by projecting a single-line laser pattern onto the GMA weld pool surface. Experimental results showed that the reflection of the single-line laser pattern could be observed, and was of convex shape.

In this paper, the revised weld pool surface measuring system for the pulsed gas metal arc welding process (GMAW-P) is demonstrated. It is capable of providing surface geometry information for the entire area of interest, i.e., the 3-D geometry of the weld pool surface. System modeling and simulation was carried out to demonstrate the principle of the potential to implement this method to reconstruct 3-D geometry of the weld pool in GMAW-P. The corresponding relationship between captured reflection pattern and original projected pattern is demonstrated. System parameters that affect observation quality are analyzed. An image processing algorithm is developed to extract and separate the reflected laser line from the captured image.

Observation System

The proposed system is shown in Fig. 1. The welding gun is fixed perpendicular to the workpiece. A 375-mW laser with 670 nm center wavelength is fixed at the backside of the welding torch. A five-line laser pattern, which is referred to as projected laser, is projected to cover the entire weld pool area. During welding progress, after the weld pool is established, specular reflection of the projected laser occurs on the weld pool surface. The reflected laser was intercepted by an imaging plane fixed vertically at the opposite side of the welding gun. The welding gun, laser pattern generator, and imaging plane are carefully aligned. The pattern shown on the imaging plane is referred to as the reflected pattern, and is captured by a high-speed camera. Raw images and enhanced images are shown in Fig. 2.

The laser pattern generator used in this study is a Coherent Powerline 670 continuous wave diode laser. The energy of projected laser is evenly distributed along each line, which ensures that the projected pattern consists of lines with uniform intensity with sharp ends. Therefore, the reflected pattern shown on the imaging plane will have relatively even intensity.

The high-speed camera is fitted with a 20-nm band-pass filter centered at the same center wavelength of the laser to enhance image contrast. Most of the arc radiation interference, which distributes on the entire wavelength spectrum, is eliminated.

The proposed reflection-based GMAW-P weld pool observation system successfully bypassed arc interference. Although the arc influence still exists, by observing the reflected laser from an imaging plane, the bright arc body is no longer part of the captured scene. Arc radiation simply functions as a close range light source that illuminates the imaging plane, resulting in a background gray level intensity. The imaging plane only contains evenly distributed arc radiation and reflected laser. Since specular reflection preserves the low-divergence character of laser, the energy of reflected laser is still concentrated. During image integration interval, as long as the energy density of reflected laser exceeds arc radiation on the intercepted area, which ensures that the reflected pattern stands out of the background, the reflected pattern can be separated. The dynamic range of the image is also fully employed because the reflected laser and the background arc light are of the same magnitude.

Reflection Image Simulation

System modeling provides a systematic tool to study the relationship between the reflected pattern and system parameters. It also helps to select optimal system parameters. It is divided into three parts: modeling of weld pool surface, modeling of projected laser, and modeling of reflection and interception.

Simulation result demonstrated that for different weld pool geometry, the resultant reflected pattern is of different shape, which suggests that the reflected pattern reveals the 3-D geometry of the weld pool surface. Meanwhile, when the weld pool surface is smooth, the height of each projected line is sequentially placed. Dynamic analysis based on simulation results demonstrates that the quality of captured images is also affected by weld pool fluctuation and camera parameters.

Modeling of Weld Pool Surface

Most current weld pool models are based on numerical analysis. The objective of such models is to evaluate how welding parameters affect weld quality, which mainly focused on the internal fluid flow and temperature distribution in the weld pool rather than the 3-D weld pool surface geometry. These models are complicated and the calculation is time consuming.

The only concern of this research is how top-side geometry of the weld pool affects laser reflection, and the consequent reflected pattern. It is not efficient to adopt existing numerical models to simulate the weld pool surface. Therefore, a simplified model based on weld pool surface geometrical appearance is selected and implemented. Although the model is not accurate, it provides fundamental understanding of the principle of the proposed observation method.

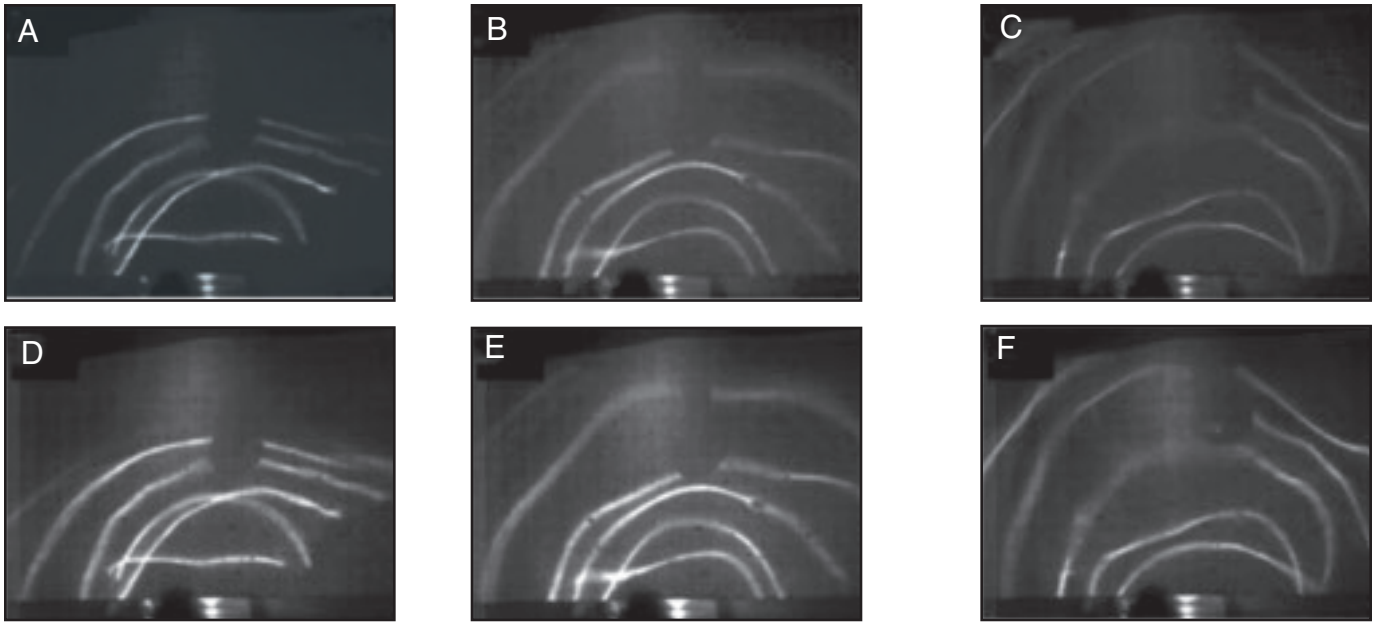

Fig. 2 — Original and enhanced images captured in bead-on-plate experiment. A, B, C — Sequential images captured in the experiment; D, E, F — Corresponding images after image enhancement.

Directly captured weld pool surface using the GMAW-P process is shown in Fig. 3. It can be observed from the captured image and solidified welding bead that the weld bead can be divided into two parts, weld pool surface and weld bead body. The weld pool surface can be estimated using part of an ellipsoid and the weld bead can be simulated using part of a cylinder. The geometry of the solidified weld specimen using designed welding parameters is measured to provide parameters for system modeling, including weld pool length, weld pool width, and weld bead height, as is shown in Fig. 4.

The weld bead is modeled using part of the cylinder. Cylinder axis is parallel to the x axis. The cylinder passes the highest point of the weld bead and the weld bead boundary on the workpiece. The function of the cylinder can be expressed as

$$F_1(x,y,z) = y^2 + (z - z_0)^2 - R^2 = 0;\ x < -l, z > 0 \quad (1)$$

The weld pool surface is simulated using part of an ellipsoid. The semi-major axis of the ellipsoid is the same as the axis of the weld bead cylinder, and the other two axes are parallel to y-axis and z-axis, respectively. Since the weld pool is continuous at all points, the weld pool model is designed to be continuous at the boundary between the partial ellipsoid and the cylinder. Ellipsoid function can be expressed as

$$F_2(x,y,z) = \frac{(x+l)^2}{a^2} + \frac{y^2}{b^2} + \frac{(z-z_0)^2}{c^2} - 1 = 0; \quad x > -l, z > 0 \quad (2)$$

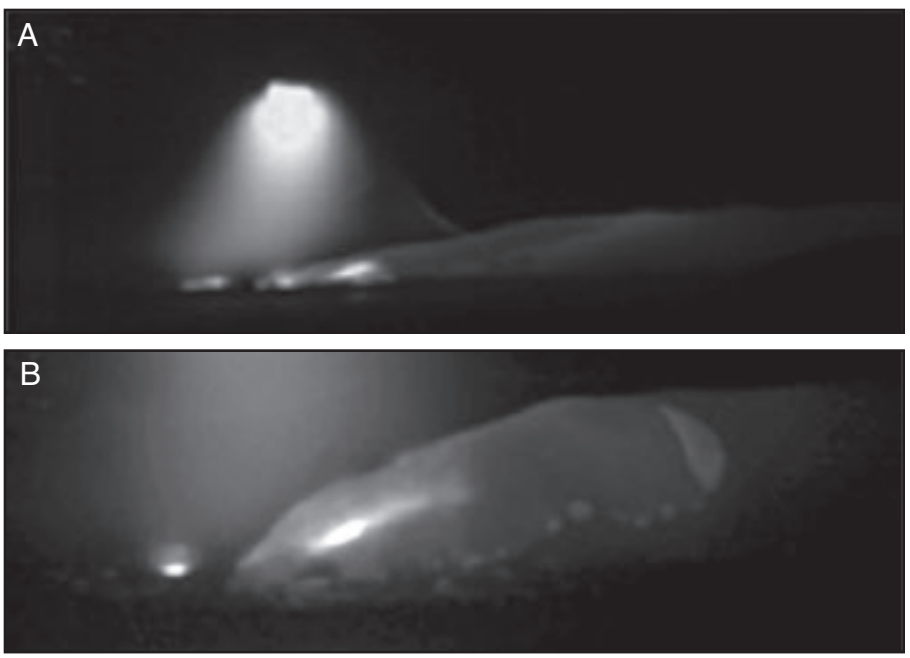

Fig. 3 — Directly captured weld pool geometry during welding process.

Therefore, the reflection surface, denoted as S, which is the actual surface where reflection occurs, can be expressed as the equation below. F_3 denotes the top side workpiece surface.

$$F_3(x,y,z) = \begin{cases} y^2 + (z - z_0)^2 - R^2 = 0 & x < -l, z > 0 \\ = \dfrac{(x+l)^2}{a^2} + & \\ \dfrac{y^2}{b^2} + \dfrac{(z-z_0)^2}{c^2} - 1 = 0 & x > -l, z > 0 \\ z = 0 \quad \text{for other points} & \end{cases} \quad (3)$$

Modeling of Projected Laser

Laser pattern generator projects a five-line parallel pattern onto the weld pool surface. It uses a refraction mechanism to split one single-line pattern to a five-line pattern. Each line is parallel with each other and every laser ray can be traced back to a single point, which is denoted as laser origin P_0.

The equation of projected laser in the universal coordinate system is determined by two fixed internal parameters, laser fan

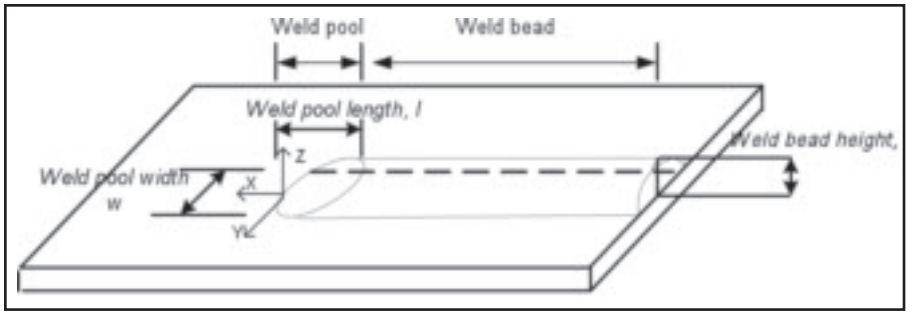

Fig. 4 — Definition of weld pool surface geometry parameters adopted in the simulation.

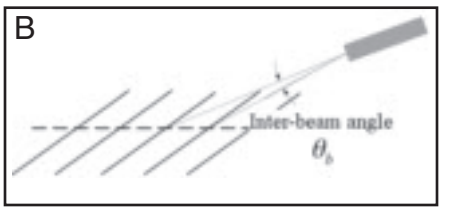

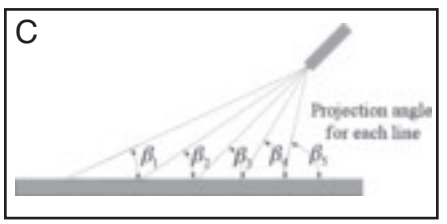

Fig. 5 — Laser angle definitions: A — Fan angle; B — interbeam angle; C — projection angle for each line.

angle θ_f, interbeam angle θ_b, and one adjustable external parameter, laser projection angle β_i for each line, as is illustrated in Fig. 5A–C, respectively.

The five-line laser pattern is projected onto the workpiece plane with each line parallel to the *y* axis. Laser origin is denoted as $P_0 = (x_0, y_0, z_0)$, the projection angle for the i th line is denoted as β_i, every ray on the i th projected laser beam can be express using the following equation:

$$\begin{cases} r = P_0 + \vec{v}\ t \\ \vec{v} = \left[\cos\theta\cos\beta_i, \sin\theta, \cos\theta\sin\beta_i\right] \\ -\theta_{fan}/2 < \theta < \theta_{fan}/2 \end{cases} \quad (4)$$

In order to reduce calculation load, each laser is replace by *n* equally spaced rays, i.e., the projected five-line laser beam is simulated using a 5-by-*n* ray matrix. The *j* th ray on the *i* th laser beam, denoted as $r_{i,j}$, can be expressed as

$$\begin{cases} r_{i,j} = P_0 + \vec{v}_{i,j}\ t, \quad t > 0 \\ \vec{v}_{i,j} = \left[\cos\theta_{i,j}\cos\beta_i, \sin\theta_{i,j}, \cos\theta_{i,j}\sin\beta_i\right] \\ \theta_{i,j}\ \dfrac{2j-n}{2n}\theta_f, \quad j = 1,2..n \end{cases} \quad (5)$$

The interception point of projected laser ray $r_{i,j}$ with weld pool surface *S*, denoted as $PW_{i,j}$, is the projected laser point on *S*, and is where reflection occurs.

Modeling of Reflected Ray and Captured Reflected Pattern

Surface *S* is composed of the weld pool surface and partial workpiece surface. Only the weld pool surface can specularly reflect the projected laser while diffuse reflection occurs on the workpiece surface. Consequently, only $PW_{i,j}$ that is on the weld pool surface will have a reflection ray, denoted as $r'_{i,j}$.

Table 1 — Maximum Line Height and Maximum Horizontal Line Span for Simulation Tests

		Test 1	Test 2	Test 3	Test 4	Test 5
Maximum line height (mm)	Line 1	14.6	31.4	62.7	—	23.6
	Line 2	38.7	46.5	70.4	22.7	47.3
	Line 3	56.2	60.1	78.4	39.7	66.1
	Line 4	72.3	73.4	87.0	54.1	84.0
	Line 5	88.5	87.1	96.0	68.3	102.7
Maximum horizontal line span (mm)	Line 1	24.5	38.5	58.0	—	36.2
	Line 2	48.4	56.2	59.4	28.6	59.3
	Line 3	63.7	68.2	61.4	42.5	76.9
	Line 4	77.4	79.5	53.9	53.7	92.6
	Line 5	90.9	90.1	67.6	64.2	108.7

The surface normal at point $PW_{i,j} = (x_{i,j}, y_{i,j}, z_{i,j})$ on surface $S = F(x,y,z)$, denoted as $n_{i,j}$ and corresponding outgoing ray, $r'_{i,j}$, can be expressed using the following equation:

$$\vec{n}_{i,j} = \left.\frac{\left(\frac{\partial F(x,y,z)}{\partial x}\right),\left(\frac{\partial F(x,y,z)}{\partial y}\right),\left(\frac{\partial F(x,y,z)}{\partial z}\right)}{\left\|\left(\frac{\partial F(x,y,z)}{\partial x}\right),\left(\frac{\partial F(x,y,z)}{\partial y}\right),\left(\frac{\partial F(x,y,z)}{\partial z}\right)\right\|}\right|_{(x_{i,j}, y_{i,j}, z_{i,j})} \quad (6)$$

The reflection of the projected laser follows the law of reflection, which states that the angle of incident ray reflection from a boundary, conventionally measured from the normal to the interface, is equal to the angle of reflection measured from the same interface. And the incident ray, the outgoing ray, and the surface normal at the interface all lie in the same plane. The outgoing ray, $r'_{i,j}$, can be expressed as

$$r'_{i,j} = PW_{i,j} + t\left(\vec{v}_{i,j} + 2\vec{n}_{i,j} \times \left(-\vec{v}_{i,j}\vec{n}_{i,j}\right)\right) \quad (7)$$

The reflected pattern captured is the interception of reflected rays by the imaging plane, which is placed parallel to the YOZ plane as is shown in Fig. 1. The distance between imaging plane and z-axis is referred to as imaging distance *d*. Since the corresponding reflected pattern from $PW_{i,j}$, denoted as $PR_{i,j} = (xr_{i,j}, yr_{i,j}, zr_{i,j})$, has a fixed x-coordinate $xr_{i,j} = d$ and is on outgoing ray $r'_{i,j}$, it can be expressed as

$$PR_{i,j} = \left(xr_{i,j}, yr_{i,j}, zr_{i,j}\right) = r'_{i,j}\Big|_{xr_{i,j}=d} \quad (8)$$

Static Simulation

Static simulation evaluates the reflected pattern when the weld pool surface is stable without any fluctuation. The objective is first to verify that each line in the reflected pattern is of a certain order so that mapping between reflected line and projected line can be established. Second objective is to evaluate the sensitivity of proposed method, i.e., how does the weld pool surface affect the reflected pattern. The third objective is to optimize system parameters.

If weld pool fluctuation is not considered, the appearance of the reflected laser is determined by the following aspect: weld pool geometry, laser projection angle, laser origin, laser fan angle, and laser interbeam angle. The last two parameters are determined by the optical characteristic of the pattern generator and cannot be adjusted.

Figure 6 demonstrates the reflected pattern generated using different weld pool geometry. The weld pool width is set

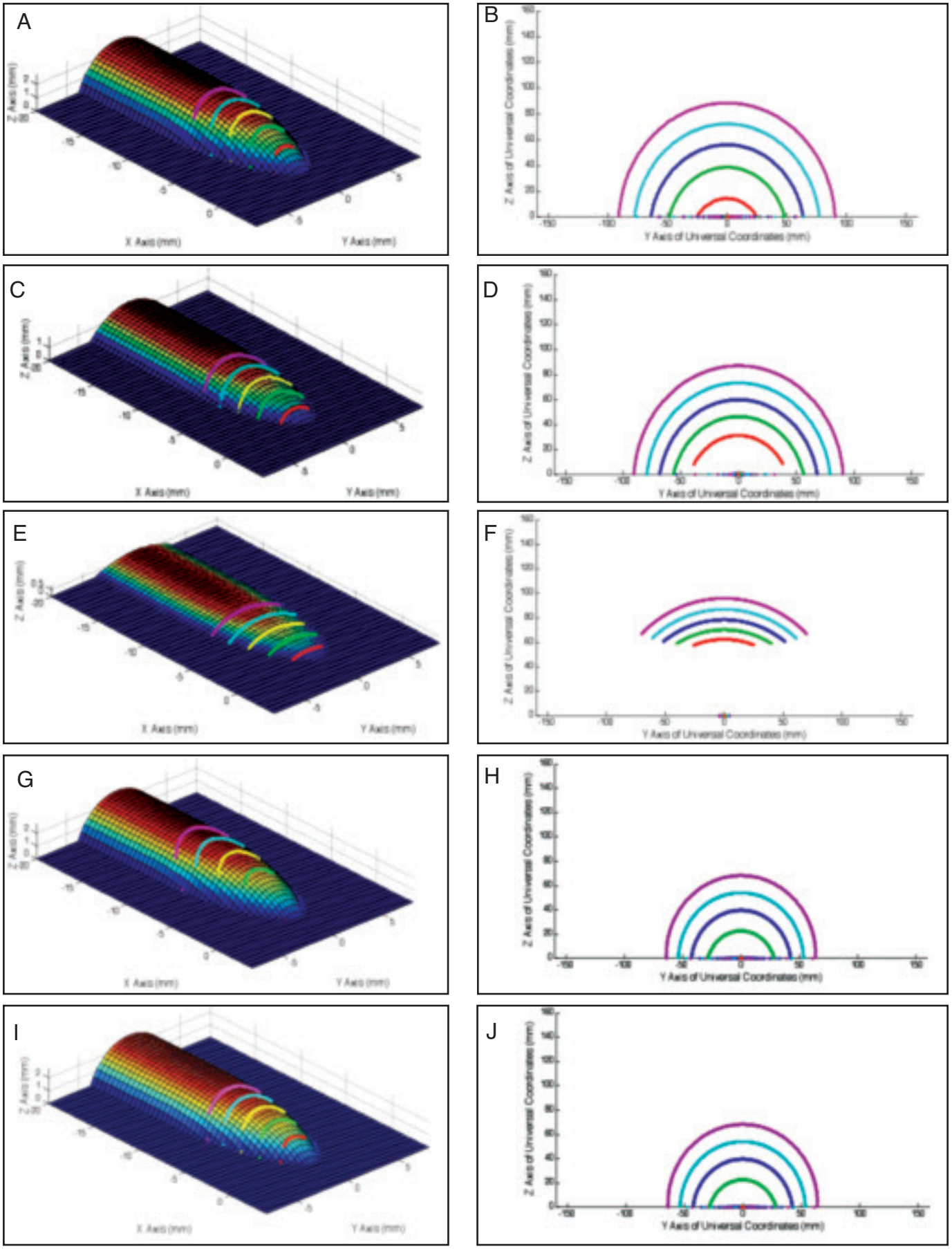

Fig. 6 — Simulation results: A — Test 1 weld pool surface; B — Test 1 reflected pattern; C — Test 2 weld pool surface; D — Test 2 reflected pattern; E — Test 3 weld pool surface; F — Test 3 reflected pattern; G — Test 4 weld pool surface; H — Test 4 reflected pattern; I — Test 5 weld pool surface; J — Test 6 reflected pattern.

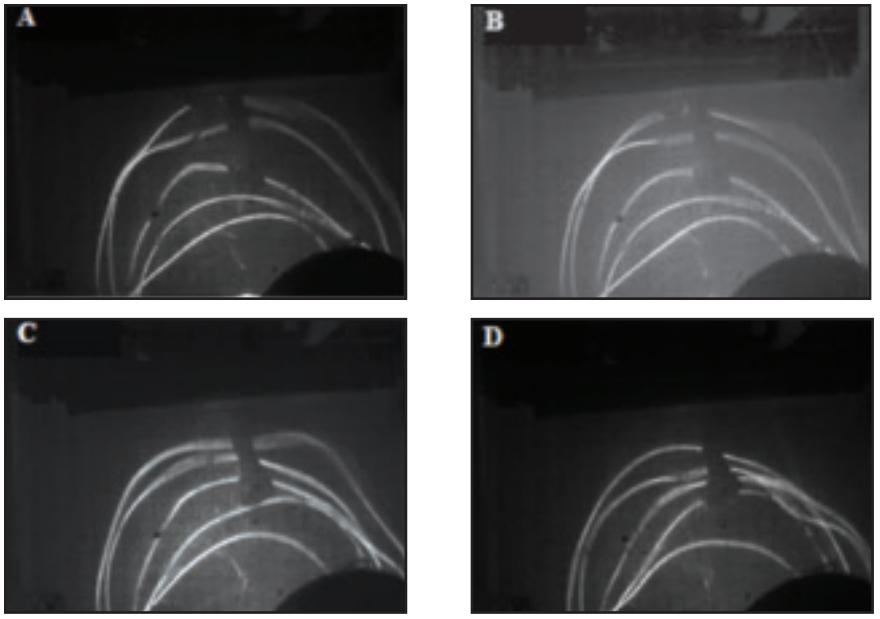

Fig.7 — Consecutive images captured in bead-on-plate experiment. Part of the imaging plane is blocked by the fixture and results in a black region in the lower-right corner of each image.

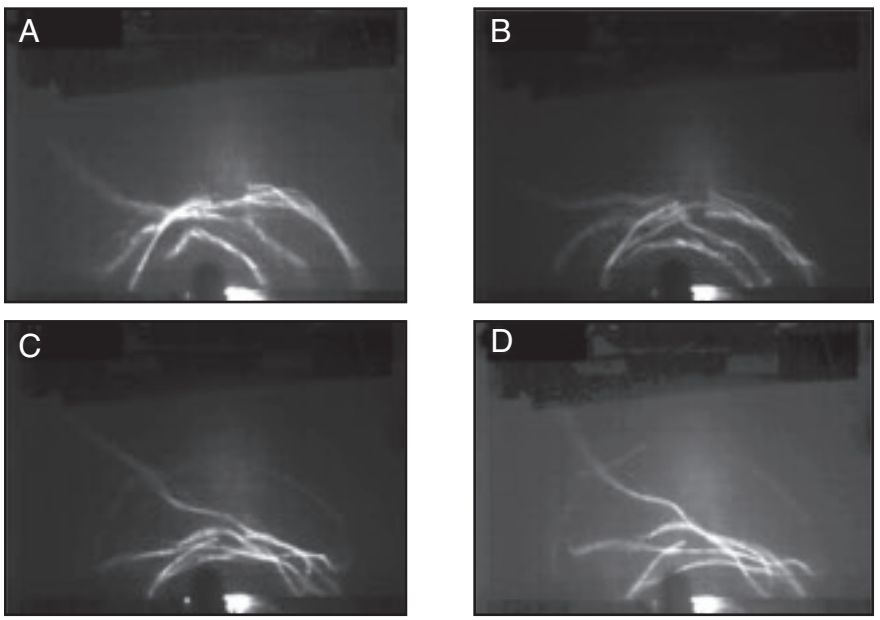

Fig. 8 — Consecutive images captured using butt joint with I-shape groove.

at 7.55 mm and the weld pool length is set as 12.75 mm in all three trials, which is measured from the solidified welding specimen. The only difference in three trials is that the weld pool surface height is decreasing, i.e. the weld pool is less convex. It is set at 2.77 mm in Test 1, which is the actual measured value, and decreases to 1.77 mm in Test 2, and 0.77 mm in Test 3. Simple statistics of the reflected line parameters, including the highest point of line, the horizontal span of each line, are demonstrated in Table 1.

Laser parameters are P_0 = (–135,0,180); laser projection angle, 55 deg; laser fan angle, 2 deg; and interbeam angle, 0.35 deg. The distance between the imaging plane and the welding gun was set at 70 mm.

Simulation results demonstrate that in all three tests, the lowest reflected line (Line 1 in Table 1) is the result of the foremost projected laser line toward the imaging plane, and the highest reflected line (Line 5 in Table 1) is the result of the laser line projected at the tail of the weld pool. Other lines are sequentially associated, which is the lower lines corresponding to the front lines, and the higher lines corresponding to the lines that are projected toward the tail of the weld pool. This result suggests that when the weld pool surface is smooth, for instance during the base current period of the GMAW-P process when the weld pool surface reaches an equilibrium status, the relationship between projected laser and reflected pattern is sequential.

It can also be observed that the reflected patterns from different weld pool geometries are distinct from each other. When the weld pool surface is relatively convex, the difference in weld pool surface geometry changes are relatively larger than that of the flatter weld pool shape. The corresponding reflected pattern spreads on the entire imaging plane. When the weld pool surface is relatively flat, which is the case when the weld pool is constrained in the I-shaped groove of a butt joint, the alternation to normal surface has minor changes. In this case, as is shown in Fig. 6F, the resultant reflected pattern is close to each other.

Tests 4 and 5 were conducted using the same weld pool surface geometry as Test 1, but with a different laser projection angle. In Test 1, the laser projection angle is set at 55 deg. It changes to 40 deg in Test 4 and 60 deg in Test 5, respectively. In order to compare with the Test 3 results, the laser origin is adjusted accordingly to ensure that in each test, the distance between each projected laser on the workpiece is kept constant. Simulation results demonstrate that the shape of the covering area of the reflected pattern increases when the laser projection angle increases.

The optimal system parameter satisfies the following conditions: Firstly, since the imaging plane is of finite dimension, the resultant reflected pattern when the weld pool is in an equilibrium state cannot exceed the predetermined imaging plane area. Secondly, the reflection angle should be determined such that the distance between each reflected line is as large as possible for easy segmentation. Thirdly, when the weld pool surface fluctuates in a small range, the resultant intercepted pattern on the weld pool surface should still be able to be identified.

Dynamic Analysis

The weld pool geometry is not the only parameter that determines the shape of the reflected pattern on the captured image. Weld pool fluctuation due to droplet impingement and arc pressure alternation severely complicated the observation. Since it is not possible to eliminate weld pool fluctuation, several other parameters must be carefully determined to

compensate for the difficulty.

Most vision-based weld pool observation methods do not address the effect camera parameters have on the quality of measurement result. However, camera setting is one of the most important parameters that determines observation results.

As a surface-normal sensitive measuring method, the rapid alternation of weld pool geometry results in a rapid change of the intercepted pattern on the imaging plane. In the ideal case, the camera frame rate is high enough so that the change of surface geometry during the integration period of one frame can be ignored. Meanwhile, laser energy density is sufficient so that on each captured image, the reflected laser pattern is distinct from that of the background arc light. In this case, when the weld pool surface geometry changes, a continuously transformed series of reflected patterns can be observed on consecutive frames, which reflect the geometry change between each integration instance. However, using one digital high-speed camera imposes certain limitations. The primary factors that affect observation results are laser energy density, camera exposure interval, lens aperture, and instant of capture.

The progress of obtaining one image can be described as follows: The scene on the imaging plane is projected onto the camera sensor plane through the lens and optical filters. During exposure interval, the camera sensor integrates the light signal that is collected on the sensor plane and the corresponding integration result is saved as captured image. If an 8-bit representation is used, such as the device we adopted in the experiment, each pixel is represented using one value from a set of integers that have only 256 different values. When the weld pool is stable during the integration interval, the appearance of the reflected pattern only has a minor change but keeps the general shape. The corresponding result is an image with a distinct reflected pattern as is shown in Fig 2. However, when the weld pool geometry changes from S_1 to S_2, according to our previous analysis, the shape of the reflected pattern will change from PR_1 to PR_2. When S_1 and S_2 are different, the corresponding motion blur due to change of scene degrades the quality of the image. Another corresponding problem caused by motion blur is that during the integration period, since the laser energy spreads on the area between patterns PR_1 and PR_2, the average laser energy on the area that reflected pattern and scanned through may not exceed the background arc light energy on the corresponding area. The contrast of the laser and background arc light is reduced. In the most severe case, the pattern is not recognizable.

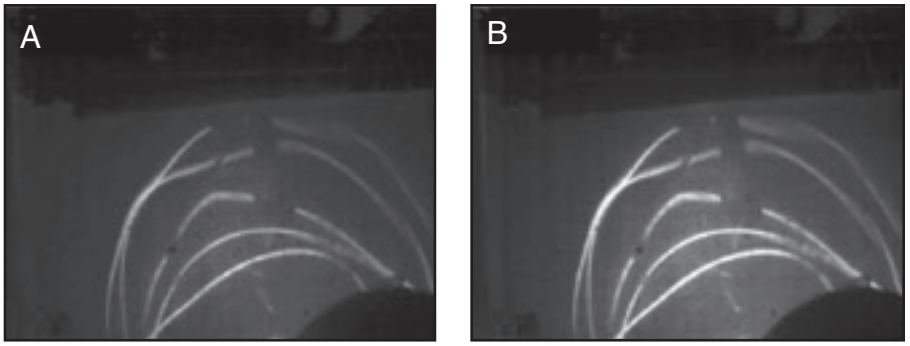

Fig. 9 — Images captured in the bead-on-plate experiment. A — Original image; B — enhanced image.

The simplest solution seems to decrease the exposure period so that the change of the reflected pattern on each image is reduced. However, with the decrease in the integration period, the total amount of light that falls onto the sensor is reduced proportionally. The low-illumination condition dramatically decreases the signal-to-noise ratio in the capture image. The integrated laser energy also reduces with the decrease in exposure period. Consequently, the difference in laser energy and background arc light is also reduced. In this case, increasing laser energy, or increasing lens aperture, which will collect more light on the camera sensor, will compensate for the cost of reducing the integration period.

Based on the experiment experience, in order to obtain a clear captured reflected pattern, the following principles should be followed:

A lens with a large aperture should be selected. A large aperture increases the total light collected on the imaging sensor, which results in a relatively bright image compared to that captured using a lens with a small aperture. Secondly, the minimum exposure interval should be determined to ensure that it is capable of capturing the change of reflected pattern that reveals surface fluctuation at required frequency. Laser energy is therefore selected based on the determined exposure interval to ensure that even if the reflected pattern has a slight alternation during the exposure interval, it will still stand out of the background.

Experiment Results

The proposed observation system was implemented to view the laser reflection from a pulsed gas metal arc welding (GMAW-P) pool surface. In the conventional GMAW process, droplets transfer from the wire onto the workpiece during the entire progress. The uncontrollable periodic droplet impingement induces severe weld pool fluctuation. A highly dynamic pool surface significantly increases observation difficulty. However, this technical difficulty can be solved by adopting a more powerful laser and camera.

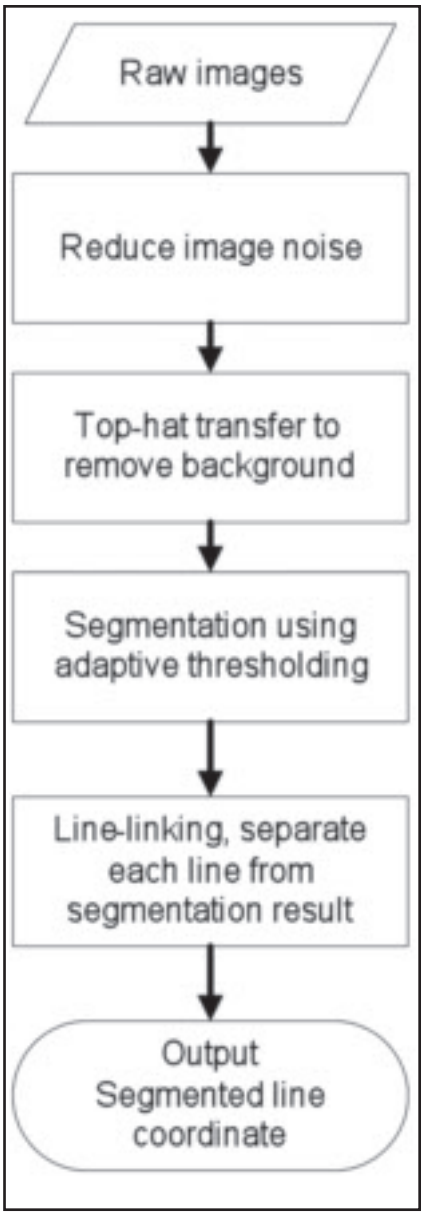

Fig. 10 — Flow chart for image processing algorithm.

Fig. 11— Result of Fig. 9 after top-hat transformation. The background is reduced.

Fig. 12 — Fig. 11 after adaptive thresholding segmentation.

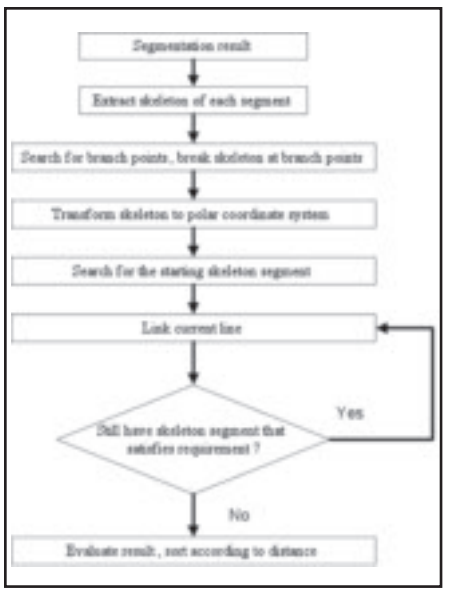

Fig. 13 — Flowchart of line-linking algorithm.

In the GMAW-P process, metal transfer only occurs during the peak current period. After the welding current switches to base current, due to reduced arc pressure and absence of droplet impingement, the external disturbance that is applied onto the weld pool is dramatically reduced. After a short period, which is typically less than 20 ms according to our observation, the weld pool surface becomes a smooth surface with relative less fluctuation. The reflected pattern captured after this period till the end of the base current period is of a regular shape and the features of reflected pattern can be extracted using image processing algorithms.

In order to demonstrate the effectiveness of the proposed method, two experiments of different weld pool geometries were conducted using the same GMAW-P parameters. The welding condition is shown in Table 2, and pulse parameters are shown in Table 3.

Images captured using a bead-on-plate experiment setup are shown in Fig. 7. This process is of partial penetration with high reinforcement. In all the images, reflected lines can be clearly identified. (The dark region in the upper-middle position that causes discontinuities in the upper three reflected lines is due to the blockage of the laser reflection by the wire and droplet.) The appearance of the reflected lines matches the simulation result shown in Fig. 6B.

An experiment using a flat butt joint with backside support was demonstrated in Fig. 8. The groove width was 1 mm. In the test, the weld pool surface is constrained in the joint, and is of relative smooth shape. The relative flat appearance of the reflected pattern coincides with the simulation result as is shown in Fig. 6F. The relative concave shape in certain images demonstrated that at that moment, the weld pool geometry was still of concave shape.

Image Processing of the Captured Reflected Pattern

The objective of the proposed weld pool observation system is to measure the 3-D weld pool geometry from the captured reflected pattern. Simulation demonstrated that reflected pattern changes when the weld pool surface geometry changes, which suggests the potential that weld pool geometry can be reconstructed from the reflected pattern. The first step is to use a segmentation method to extract the line pattern.

A typical raw image captured at base current period is shown in Fig. 9A. An enhanced image using contrast stretching is shown in Fig. 9B in order to better demonstrate the property of the raw image. It can be observed that the captured raw images contain significant noise and uneven background intensity. Due to weld pool surface fluctuation, certain lines in the reflected pattern may intercept or overlap with each other. One reflected line also might appear as several discontinuous segments rather than a single continuous line. The contrast between laser pattern and background arc light might be low in certain areas, for instance at the upper right part in Fig. 9, and certain lines might be much wider than others.

A robust feature extraction algorithm

Table 2 — Welding Condition

Base Metal	10-mm Mild Steel
Wire diameter	1.2 mm
Shielding gas	Argon
Gas flow	20 L/min
Welding speed	5 mm/s
Wire feeding speed	130 in./min
Contact-tube-to-workpiece distance	22 mm

Table 3 — Pulse Parameters

Average welding current	115 A
Peak current	220 A
Base current	50 A
Pulse frequency	10 Hz
Peak current duration	38.2 ms
Base current duration	61.8 ms

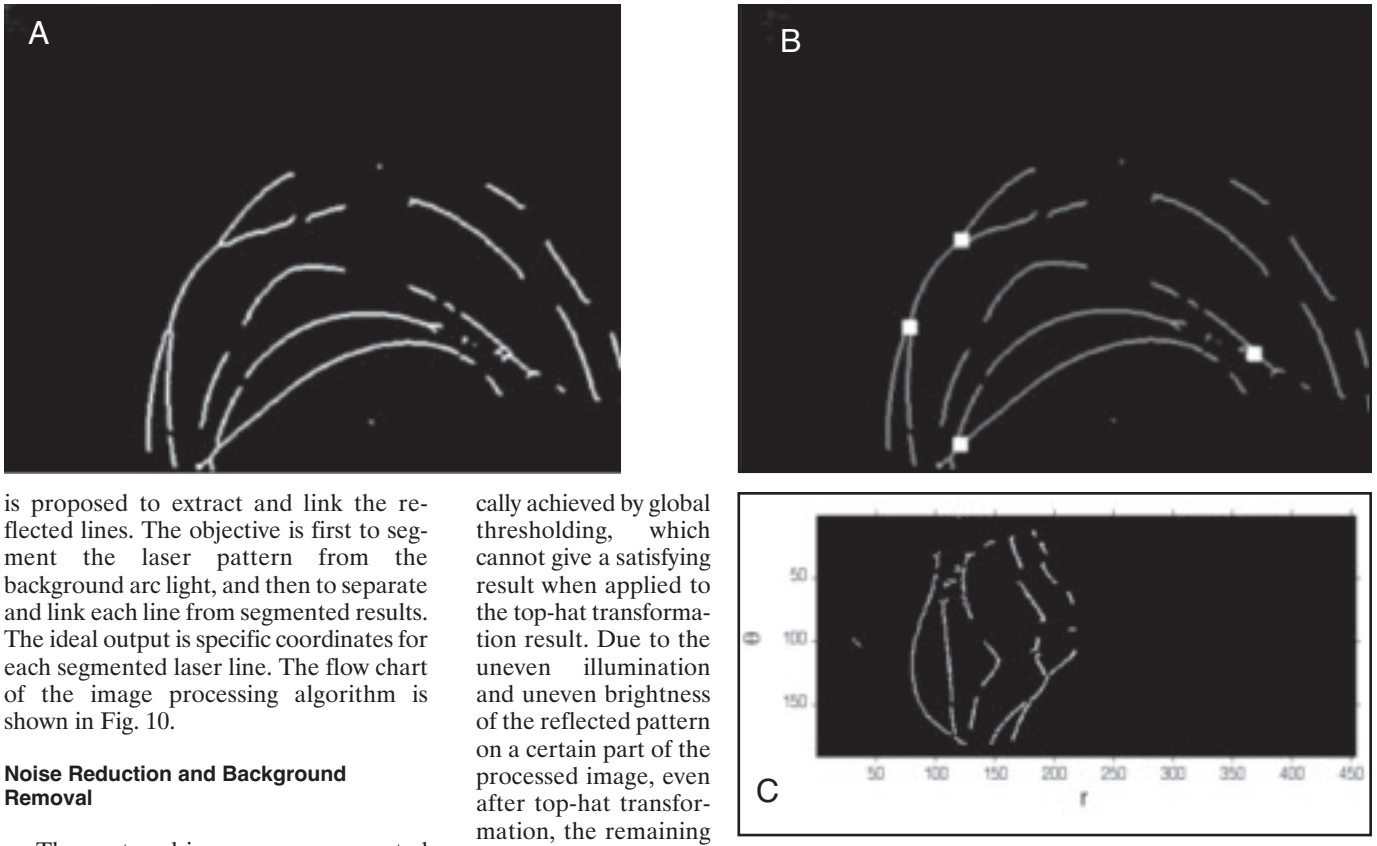

Fig. 14 — Morphological operation and coordination transformation. A — Skeleton of segmentation results; B — marked interception points; C — skeleton in polar coordination system.

is proposed to extract and link the reflected lines. The objective is first to segment the laser pattern from the background arc light, and then to separate and link each line from segmented results. The ideal output is specific coordinates for each segmented laser line. The flow chart of the image processing algorithm is shown in Fig. 10.

Noise Reduction and Background Removal

The captured images were generated using low exposure time, large aperture, and under insufficient illumination, which inevitably introduced noises that degraded the image. A frequency domain Gaussian low-pass filter as described in Equation 9 was applied to smooth the obtained image and remove noise.

$$H(u,v) = e^{-D^2(u,v)/D_0^2} \qquad (9)$$

The background arc light is unevenly distributed. As can be observed, it is of greater value at the lower center of the imaging plane, which is closer to the arc, than at other parts of the image. A morphological top-hat transformation (Ref. 9) is proposed to remove background and increase contrast between the reflected laser pattern and background. It is achieved by first obtaining a gray-scale opening of the image by one 7 × 7 structuring element, and then subtracting it from the original image. The corresponding result is shown in Fig. 11. It can be observed that the contrast between the laser and background is dramatically enhanced, especially at the upper area where the contrast on the original image is relatively low.

Reflected Image Segmentation — Adaptive Thresholding

Segmentation subdivides the obtained image into its constituent regions of reflected pattern and background arc light, and extracts one of the regions. It is typically achieved by global thresholding, which cannot give a satisfying result when applied to the top-hat transformation result. Due to the uneven illumination and uneven brightness of the reflected pattern on a certain part of the processed image, even after top-hat transformation, the remaining background intensity still exceeds the darkest reflected pattern on the other area.

In this application, the decision whether to segment a pixel as a reflected pattern or background is only determined by its neighboring pixels. Therefore, adaptive thresholding was adopted, which first divided the original image into square blocks, then assigned different thresholds to each block. To reduce segmentation error, blocks were divided in such a way that for each pair of neighboring blocks, 50% of their area overlapped with each other.

The adaptive thresholding algorithm can be described as follows: for every pixel (x,y) in the captured image, its gray value is denoted as $f(x,y)$. Background pixels are denoted as B and reflected pattern was denoted as PW. The average gray level in the i th block, which contains pixel (x,y) is denoted as μ_i and the threshold is described as $T_i = \mu_i + \Delta T$. Then, we will have

$$\begin{cases} (x,y) \in B_i, & f(x,y) < T_i \\ (x,y) \in PW_i, & f(x,y) \geq T_i \end{cases} \qquad (10)$$

One pixel was treated as a reflected pattern only when it was determined to be part of the reflected pattern in more than three different blocks. The corresponding segmentation result is shown in Fig. 12, which gives a clear segmentation with little noise.

Line Linking

As can be observed in Fig. 12, in the segmentation results, the reflected lines are not necessarily distinct continuous lines as is the simulation results shown in Fig. 6. In certain areas, the reflected lines intercept or even overlap with each other. Gaps between line segments, which is due to electrode blockage of the reflected laser or insufficient contrast between the reflected pattern and the background, also exist.

The basic principle for the line-linking algorithm is that each line can be modeled as a continuous arc. If we define a point $O(x_0,y_0)$ at the captured image, the arc equation $f(x,y) = 0$ can be expressed in a polar coordinate system, which has O as pole and y^+ as polar axis, as $g(r, \theta) = 0$. If we travel along each line, both θ and r are continuous.

Both simulation and experimental results demonstrated that the arc is of a convex shape, therefore, if the pole is selected at the center bottom of the captured image, every segment on the same line can be clustered by utilizing the continuous characteristic of θ and r.

The line-linking algorithm is divided into seven steps. The flow chart is shown

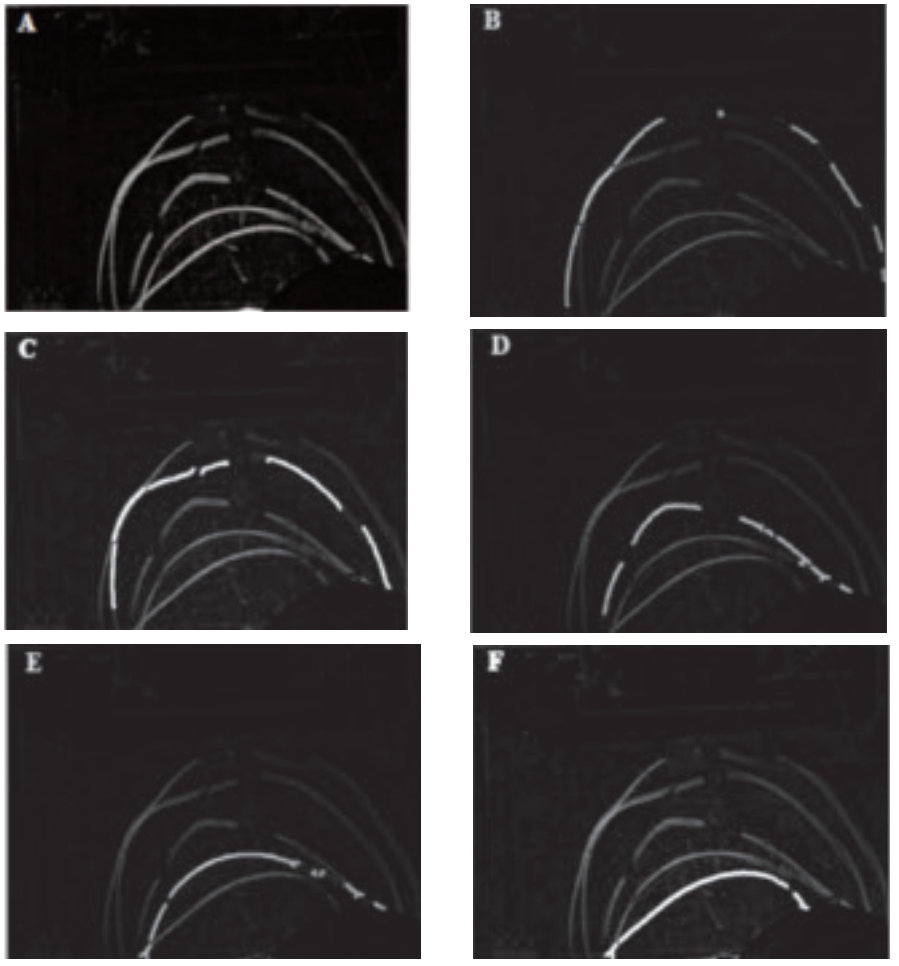

Fig. 15 — Line extraction results. A — Original image; B — extracted line 1; C — extracted line 2; D — extracted line 3; E — extracted line 4; F — extracted line 5.

in Fig. 13. Each segment is first represented using its morphological skeleton to reduce redundant information and reduce calculation load, as is shown in Fig. 14A. Branch points in the skeleton, at the interception points of different lines, are located and removed, as is shown in Fig. 14 B. Each skeleton branch is labeled and then transformed into a polar coordinate, as is shown in Fig. 14C.

Line linking in the polar system starts from segments, which have relatively larger elements, located at the center of the image, and having a larger r value. It follows the angle and distance continuity characteristic of the line, which means the search for the next candidate is along the θ axis. The difference in r between two neighboring segments must not exceed a certain threshold. When all the segments that are larger than a certain threshold have been clustered, the segmentation clustering result is evaluated and each line is sorted based on its average r. From the simulation result, it can be assumed that the fifth line has the largest r and the first line has the smallest r.

Segmentation results in both the polar coordinate system and the original image are shown in Fig. 15. The segmented and linked reflected lines created a foundation for future reconstruction of the weld pool surface.

Conclusion

The proposed system, which projects a five-line pattern onto the weld pool surface and observes its reflection on an imaging plane, provides an effective method to monitor specular GMAW-P pool surface.

System modeling and simulation have been used to help find appropriate ranges of the parameters in the imaging system elements to successfully image the laser pattern reflected from the weld pool surface in GMAW-P.

System modeling and simulation also demonstrated that the observed imaging plane pattern reflects 3-D geometry of GMAW-P weld pool surface. As a surface-normal sensitive measuring method, the reflected pattern is sensitive to weld pool surface fluctuation, which in severe cases will significantly degrade observation results, which is defined as whether clear line reflection is present on the captured image.

Dynamic analysis demonstrated that the quality of captured images is also determined by laser energy density and camera parameters. The effect of weld pool fluctuation can be compensated by increasing laser energy, increasing camera lens aperture, to reduce the image integration interval.

Corresponding analysis demonstrated that when the weld pool is relatively smooth, which is similar to the weld pool shape at the equilibrium state at the base current period in GMAW-P, the intercepted laser lines can be sequentially matched with projected lines.

Each individual reflected line can be automatically separated from the captured image using the proposed image processing algorithm.

The proposed method forms a systematic approach to acquire data for future reconstruction of the GMAW-P weld pool surface.

Acknowledgments

This research was funded by the National Science Foundation under grant CMMI-0726123 entitled Measurement and Control of Dynamic Weld Pool Surface in Gas Metal Arc Welding.

References

1. Rokhlin, S. I., and Guu, A. C. 1990. Computerized radiographic sensing and control of an arc welding process. *Welding Journal* 69: 83-s to 97-s.

2. Richardson, R. W. 1984. Coaxial arc weld pool viewing for process monitoring and control. *Welding Journal* 63(3): 43–50.

3. Kovacevic, R., Zhang, Y. M., and Ruan, S. 1995. Sensing and control of weld pool geometry for automated GTA welding. *Journal of Engineering for Industry-Transaction of the ASME* 117(2): 210–222.

4. Minch, C. 2004. Development of a synchronized, high-speed, stereovision system or in situ weld pool measurement. Master's thesis. Golden, Colo., Colorado School of Mines.

5. Zhao, D. B., Yi, J. Q., et al. 2003. Extraction of three-dimensional parameters for weld pool surface in pulsed GTAW with wire filler. *Journal of Manufacturing Science and Engineering* 125: 493–503.

6. Kovacevic, R., and Zhang, Y. M. 1996. Sensing free surface of arc weld pool using specular reflection principle and analysis. *Proceedings of the Institution of Mechanical Engineers, Part B, Journal of Engineering Manufacturing* 210(6): 553–564.

7. Song, H. S., and Zhang, Y. M. 2008. Measurement and analysis of three-dimensional specular gas tungsten arc weld pool surface. *Welding Journal* 87(4): 85-s to 95-s.

8. Ma, X., and Zhang, Y. M. 2009. Reflection of illumination laser from gas metal arc weld pool surface. *Meas. Sci. Technol* 20(11).

9. Gonzalez, R. C., and Woods, R. E. 2002. *Digital Image Processing*, 2nd Edition. Prentice Hall.